Quantification of Spin Drift in Devices with a Heavily Doped Si Channel

A. Spiesser,[1,*] Y. Fujita,[1] H. Saito,[1] S. Yamada,[2,3] K. Hamaya,[2,3] W. Mizubayashi,[4] K. Endo,[4] S. Yuasa,[1] and R. Jansen[1]

[1]*Spintronics Research Center, National Institute of Advanced Industrial Science and Technology (AIST), Tsukuba, Ibaraki 305-8568, Japan*
[2]*Department of Systems Innovation, Graduate School of Engineering Science, Osaka University, Toyonaka 560-8531, Japan*
[3]*Center for Spintronics Research Network, Graduate School of Engineering Science, Osaka University, Toyonaka 560-8531, Japan*
[4]*Nanoelectronics Research Institute, National Institute of Advanced Industrial Science and Technology (AIST), Tsukuba, Ibaraki 305-8568, Japan*

(Received 9 December 2018; revised manuscript received 17 February 2019; published 8 April 2019)

The effect of a drift electric field on the spin transport in a heavily doped Si channel is investigated using nonlocal devices. A simple method to accurately quantify spin drift is established, using the ratio of the nonlocal spin-valve signal for two measurement configurations that have a different electric field pattern in the channel. The spin-transport length is obtained as a function of the electric field, and it is found that in heavily doped Si, drift electric fields of ±400 V/cm modify the spin-transport length (either up or down) by about a factor of two, relative to the length scale for purely diffusive transport. Although the trends are in agreement with the theory for spin drift, a quantitative comparison reveals that the theory significantly overestimates the effect of spin drift (by a factor of three). This highlights that an accurate experimental quantification of spin drift, as provided here, is crucial for a correct assessment of the role and importance of spin drift in practical spin-transport devices.

DOI: 10.1103/PhysRevApplied.11.044020

I. INTRODUCTION

Silicon, owing to its advanced technology maturity and large spin lifetime and spin-diffusion length, represents an ideal semiconductor (SC) material to design and fabricate alternative logic devices that employ the spin functionality [1–6]. Understanding the fundamental physics of spin transport in Si is crucial to successfully implement Si spintronic devices in future information processing technologies. To date, the most practical method to achieve spin injection in Si-based devices consists of driving a current from a ferromagnetic (FM) tunnel contact into the Si [5–12]. Due to spin-polarized tunneling [13,14], this induces a spin accumulation in the nonmagnetic Si, which is characterized by a splitting $\Delta\mu$ of the electrochemical potential of spin-up and spin-down electrons. FM tunnel contacts are also suitable to effectively convert the spin accumulation into a charge voltage [15–17]. Using this approach, all-electrical spin injection, transport, and spin detection have been demonstrated in Si channels using the nonlocal four-terminal geometry [7,9–12,17]. Notably, the creation of a giant spin accumulation in a heavily-doped Si channel from Fe/MgO tunnel contacts has recently been reported [12], making this an ideal system to study spin-dependent transport in Si.

The equations [1,2] that describe the transport of spins in a nonmagnetic channel include spin diffusion, but also spin drift due to the electric field associated with a charge current in the channel [18,19]. If the charge current density in the channel is small, the spin transport is described well by taking only spin diffusion into account, and the spatial decay of the spin accumulation is governed by the spin-diffusion length L_{SD}. At larger drift electric fields, spin drift starts to play a role, and it modifies the spin-transport length, either increasing or decreasing it, depending on whether the spin drift drives spins in the same direction as spin diffusion or in the opposite direction [18,19].

An accurate quantification of spin drift is then required for two reasons. First, in many practical spin-transport devices [1–5], a charge current is present in the region where spin transport occurs. A notable example is the two-terminal magnetoresistance device consisting of a semiconductor channel and two FM contacts [16], in which a current is applied between the two FM contacts, and thus a drift electric field exists in the channel between the two contacts. Quantification of the role of spin drift is thus important for understanding the device characteristics and performance, and spin drift may be used to enhance the

*aurelie.spiesser@aist.go.jp

magnetic response. Second, the analysis of spin-transport data and the extraction of spin-transport parameters, such as the spin polarization of the injected current, rely on a precise theoretical description of the spin transport, which, in general, has to include spin drift.

Yu and Flatté [18,19] derived an expression for the spin-transport length that includes the effect of spin drift starting from the drift-diffusion equation for spin polarization in semiconductors. Assuming a homogeneous SC material without space charge, the expression for the up-spin (down-spin) electron density $n_{\uparrow(\downarrow)}$ in the SC is given by

$$\nabla^2(n_\uparrow - n_\downarrow) + \frac{\mu E}{D}\nabla(n_\uparrow - n_\downarrow) + \frac{1}{(L_{\mathrm{SD}})^2}(n_\uparrow - n_\downarrow) = 0, \tag{1}$$

with μ the mobility, D the diffusion constant of the channel material, and E the drift electric field in the channel. The latter is determined by the current density J_{SC} in the channel and the channel resistivity ρ_{SC} via $E = \rho_{\mathrm{SC}} J_{\mathrm{SC}}$. From Eq. (1), one obtains [18,19] the spin-transport length $L(E)$ that depends on the drift electric field E in the SC channel as

$$L(E) = \left(\frac{eE}{2\varepsilon_d} + \sqrt{\left(\frac{eE}{2\varepsilon_d}\right)^2 + \left(\frac{1}{L_{\mathrm{SD}}}\right)^2}\right)^{-1}, \tag{2}$$

where e is the elementary charge and the parameter $\varepsilon_d = eD/\mu$ is an energy scale that controls the strength of the spin drift [note that we have defined the sign of the electric field to be positive when it is directed against the spin diffusion (upstream) and negative when it is in the same direction as the spin diffusion (downstream)]. When a significant drift electric field is present, the spin accumulation is transported through the SC channel over distances significantly larger (downstream electric field) or smaller (upstream) than the spin-diffusion length L_{SD}.

Experimentally, the effect of electric fields has been investigated in devices with different channel materials. In graphene-based devices [20], spin drift was shown to change the spin-valve signals by as much as 50% for drift electric fields up to 700 V/cm applied to the channel between the injector and detector FM contacts. In GaAs-based devices, it was reported that a bias current in the detector circuit causes modulation of the spin-detection efficiency [21]. Although this was originally interpreted as being due to spin drift, measurements at lower current densities [22] led the same authors to conclude that spin drift is not responsible. In fact, it was recently shown that modulation of the spin-detection efficiency by a bias across the detector originates from the nonlinearity of the tunnel transport [17]. In devices with a nondegenerate Si channel [23,24], for which spin drift is expected to be significant, clear effects of spin drift were indeed observed, including significant enhancements of the spin-transport length. For Si-based devices with a heavily doped Si channel, the presence of spin drift was also convincingly demonstrated [25] by comparing spin signals in the local and the so-called crossed nonlocal geometry (see below and Fig. 1). However, for the quantification of spin drift, the authors used the Hanle signals, which is not reliable, as we explain in the Supplemental Material [26,27]. The results reported in Ref. [28] suffer from the same issue.

Here, we study how a drift electric field in a heavily doped Si channel changes the spin transport. We compare the magnitude of the spin-valve signals observed in nonlocal devices in the conventional nonlocal measurement configuration with those measured in a modified, crossed nonlocal scheme having a different electric field pattern in the channel. It is shown that from the ratio of the spin signals in those two configurations, the spin drift can be accurately quantified. We obtain the spin-transport length $L(E)$ as a function of E and extract the value of the energy scale ε_d that governs spin drift from the data. We find that the experimental energy scale is significantly larger (by a factor of three) compared to what is expected from the theory ($\varepsilon_d = eD/\mu$), implying that the theory significantly overestimates the effect of spin drift. We also demonstrate that spin drift changes the magnitude of the spin accumulation that is detected in the conventional nonlocal geometry, even though there is no electric field in the channel between the injector and detector. Therefore, we introduce a spin drift correction factor in the expression for the nonlocal spin-valve signals, which is important when parameters, such as the spin polarization of the injected current, are extracted from the magnitude of the nonlocal spin-valve signal at larger bias. Note that the phenomenon

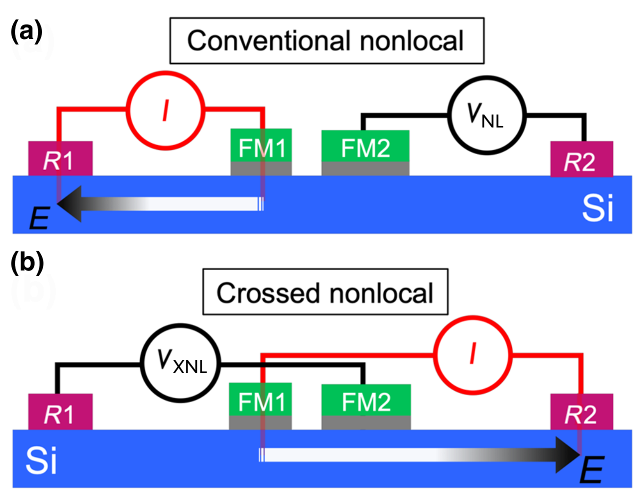

FIG. 1. Schematic diagrams of the four-terminal nonlocal device, with the circuit configuration for (a) the conventional nonlocal (NL), and (b) the crossed (XNL) measurements.

of spin drift due to a charge current in the channel, as studied here, is completely different from the effect of a bias voltage across the detector tunnel contact, which, as we recently reported [17], produces a nonlinear spin detection that originates from the tunnel transport in the detector.

II. QUANTIFICATION OF SPIN DRIFT IN NONLOCAL DEVICES

To evaluate the contribution of spin drift in nonlocal devices, we employ two different circuit configurations, hereafter called conventional nonlocal (NL) and crossed nonlocal (XNL) geometries, as illustrated in Fig. 1. For the NL geometry [Fig. 1(a)], a constant current I is applied from FM1 to a first reference contact ($R1$) and a spin signal is detected by probing the voltage between FM2 and a second reference contact ($R2$). Consequently, an electric field is present in the injector circuit, but not in the detector circuit or in the channel between the injector and detector. For the XNL configuration [Fig. 1(b)], I is applied between FM1 and $R2$ and the voltage is probed between FM2 and R1. Thus, in the XNL scheme, the direction of the current in the channel, and therefore the electric field, are in the opposite direction, and the electric field is present between the injector and the detector. However, note that in both configurations there is no tunnel current across the FM/Si detector junction (FM2), and that the current across the injector tunnel contact (FM1) is chosen to be the same for both configurations. Hence, only the electric field pattern in the Si channel is modified. In Fig. 2, we present the schematic diagrams with the corresponding spin accumulation profiles in the Si channel under different bias conditions. In the low-bias regime [Fig. 2(a)], the spin transport is dominated by spin diffusion and spin drift is negligibly small. As a consequence, the spin accumulation profile in the Si channel is identical for the NL and XNL configurations. The spin accumulation $\Delta\mu$ is maximal at the center of the injector and decays symmetrically in both directions due to the isotropic spin diffusion in the Si channel, with a decay length given by L_{SD}. In this purely diffusive regime, the NL spin signal (V_{NL}) for both configurations can be expressed as

$$V_{\mathrm{NL}} = P_{\mathrm{inj}} P_{\mathrm{det}}\, J_T \rho_{\mathrm{Si}}\, L_{\mathrm{SD}} \left(\frac{W_{\mathrm{inj}}}{2t_{\mathrm{Si}}}\right) \exp\left(\frac{-d_c}{L_{\mathrm{SD}}}\right), \quad (3)$$

with J_T the tunnel current density across the injector tunnel contact, P_{inj} the spin polarization of the injected tunnel current, P_{det} the spin-detection efficiency of the detector contact, ρ_{Si} the resistivity, t_{Si} the thickness of the Si channel, W_{inj} the width of the injector contact, and d_c the center-to-center distance between the injector and detector contacts. This expression is accurate [12] when the width of the FM contacts is smaller than L_{SD} (line injector approximation), and applies to devices for which t_{Si} is small compared to L_{SD}.

In the high-bias regime, the presence of a non-negligible electric field in the channel induces spin drift, which causes an asymmetric distribution of the spin accumulation on the two sides of the spin injector. This effect is illustrated in Figs. 2(b) and 2(c) for high-bias spin injection and spin

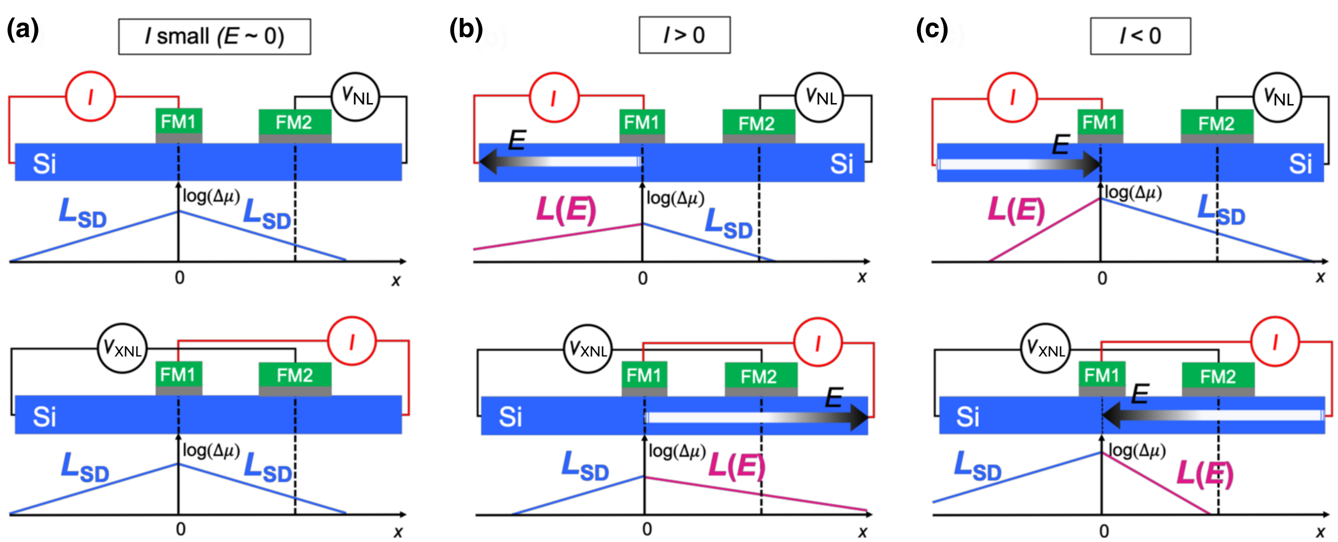

FIG. 2. Schematic diagrams of the Si nonlocal devices with the corresponding spin accumulation profiles in the Si channel at (a) low current, (b) large spin injection bias, and (c) large spin extraction bias. The top and bottom panels correspond to the conventional nonlocal and the crossed-nonlocal measurement configurations, respectively. When the electric field is absent or negligibly small, the spin accumulation decays due to spin diffusion only (blue solid lines, label L_{SD}), whereas in the presence of a strong E, the spin signal decays due to spin drift and spin diffusion [magenta solid lines, label $L(E)$]. The horizontal axis corresponds to the distance x from the center of the injector, whereas the vertical axis corresponds to the logarithm of the spin accumulation.

extraction conditions, respectively. For the conventional NL configuration, a large spin injection bias [Fig. 2(b), top panel], enhances the spin-transport length to a value $L(E) > L_{SD}$ on the left side of the injector, whereas the decay on the right side is still determined by L_{SD}, since there is no electric field there. However, for the XNL configuration [Fig. 2(b), bottom panel], a large spin injection bias enhances the spin-transport length on the right side of the injector where the electric field is present, whereas the decay on the left side is determined by L_{SD}. For a large spin extraction bias [Fig. 2(c)], a similar asymmetry is introduced, but now the electric field has the opposite polarity and thus reduces the spin-transport length (on the left side of the injector for the NL configuration and on the right side of the injector for the XNL configuration, respectively).

If the tunnel current across the injector contact is chosen to be identical for the NL and XNL configurations, all the parameters that determine the detected nonlocal spin signal are the same except for the exponential decay term. Thus, it directly follows that the ratio of the spin signals V_{XNL} and V_{NL} in the XNL and NL configurations, respectively, is given by

$$\frac{V_{XNL}}{V_{NL}} = \frac{\exp\left(\frac{-d_c}{L(E)}\right)}{\exp\left(\frac{-d_c}{L_{SD}}\right)}. \tag{4}$$

The ratio is larger than 1 for spin injection bias and smaller than 1 for spin extraction bias. Since the value of L_{SD} can be obtained from regular nonlocal spin-transport measurements, the spin-transport length $L(E)$ as a function of E can be obtained directly from a measurement of the ratio between V_{XNL} and V_{NL} in a single device. The described method allows one to precisely quantify the spin-transport length as a function of E without having to determine the variation of P_{inj} and P_{det} as a function of the bias current.

III. GROWTH AND DEVICE FABRICATION

The Si nonlocal devices [Fig. 3(a)] are fabricated on a silicon-on-insulator substrate having a 70-nm thick n type Si(001) channel on the top of the buried oxide. The Si channel is doped with phosphorous using ion implantation. The properties of the Si channel are characterized using a Hall bar structure that is simultaneously fabricated with the nonlocal devices. From this, the carrier concentration n, the resistivity ρ_{Si}, and the mobility μ of the Si channel are measured to be 7.6×10^{18} cm^{-3}, 5.6 mΩ cm, and 147 cm^2/V s at 60 K, respectively. Prior to the deposition of the FM tunnel contact, the Si substrate is chemically cleaned following the so-called RCA method described in Ref. [12]. The substrate is then annealed in the ultra-high vacuum molecular beam epitaxy system at 700 °C for 10 min. After this step, *in situ* reflection high-energy

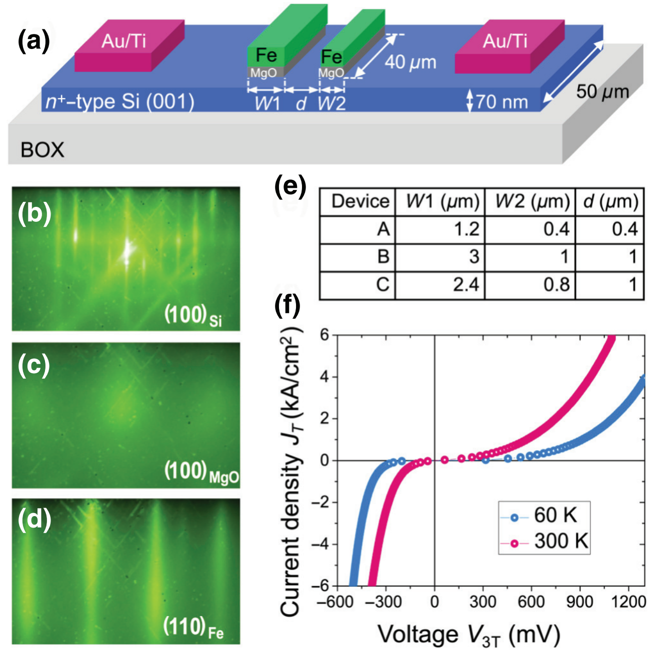
(e)

Device	$W1$ (μm)	$W2$ (μm)	d (μm)
A	1.2	0.4	0.4
B	3	1	1
C	2.4	0.8	1

FIG. 3. (a) Schematic layout of the nonlocal device with relevant dimensions indicated. (b–d) RHEED patterns of (b) the $c(2 \times 4)$ surface reconstruction along the [100] azimuth of the Si after *in situ* annealing at 700 °C, (c) the MgO(001) layer along the [100] azimuth of the MgO, and (d) the Fe(001) layer along the [110] azimuth of the Fe. (e) Geometric parameters of the three devices A, B, and C used in this study. Given are the widths $W1$ and $W2$ of the ferromagnetic tunnel contacts, and the gap d between the two contacts. Note that the center-to-center distance d_c is given by $d + (W1 + W2)/2$. (f) Tunnel current density J_T as a function of bias voltage V_{3T} for the 0.4 μm wide FM tunnel contact of device A, measured in a three-terminal configuration at 60 and 300 K.

electron diffraction (RHEED) displays intense and sharp $c(2 \times 4)$ streaks, confirming a very clean and smooth Si surface, as shown in Fig. 3(b). The MgO tunnel barrier is deposited using a two-step method, which consists of the deposition of 0.5 nm of MgO at 80 °C followed by the deposition of 1 nm of MgO at 300 °C. This results in spotty RHEED patterns corresponding to crystalline MgO(001) [Fig. 3(c)]. Then, a 10-nm thick Fe layer is deposited at 100 °C, followed by a postannealing at 250 °C for 5 min, leading to streaky RHEED patterns as shown in Fig. 3(d). Finally, a 20-nm thick Au capping layer is grown at room temperature. The sample is processed into four-terminal Si lateral devices using standard microfabrication techniques (e beam lithography, Ar-milling, SiO_2 sputtering). The width of the FM contacts and the spacing of the devices used in this study are summarized in Fig. 3(e). The electronic transport properties of the tunnel contacts are measured in a three-terminal configuration. As shown in Fig. 3(f), the current-density vs voltage (J_T-V) characteristics are strongly nonlinear and asymmetric at both 60 and 300 K. Due to the use of a relatively thick MgO tunnel barrier (approximately 1.5 nm), the interface resistance of the tunnel barrier is larger than $10\,\mathrm{k}\Omega\,\mu\mathrm{m}^2$ over the complete range of biases used in the experiments. This is much larger than the effective spin resistance of the Si channel ($r_{\mathrm{Si}} \sim 2\,\mathrm{k}\Omega\,\mu\mathrm{m}^2$), so that there is negligible backflow of the spins from the Si into the FM contact [2,16]. Although spin signals are clearly observed up to 300 K, all the measurements presented in this study are performed at 60 K, repeated several times, and then averaged to improve the signal-to-noise ratio, allowing a better estimation of the spin transport parameters. The nonlocal spin-valve and Hanle-type spin precession measurements are obtained by applying an external magnetic field along the length of the FM contacts (B_y) (i.e., along the y axis) and perpendicular to the film plane (B_z), respectively. A positive (negative) current corresponds to electron injection from the Fe into the Si (electron extraction from the Si to the Fe).

IV. SPIN TRANSPORT IN THE DIFFUSIVE REGIME

We first determine the basic spin-transport parameters of the device in the very low-bias regime, where the spin-transport can be described as purely diffusive. Figure 4(a) shows the nonlocal spin-valve measurement obtained at a temperature (T) of 60 K on device A using the 1.2-μm wide FM contact as the spin injector and the 0.4-μm wide FM contact as the nonlocal detector. The tunnel current density across the injector interface J_T is approximately 0.8 kA/cm^2 ($I = 0.4$ mA), which corresponds to a negligibly small electric field in the Si channel ($E \sim 60$ V/cm). A typical spin-valve behavior is observed with sharp switching between parallel (P) and antiparallel (AP) configurations of the magnetization of the injector and detector. The magnitude of the nonlocal spin signal (V_{NL}) is approximately 0.22 mV, which corresponds to a spin-resistance area product spin-$RA = A\ V_{\mathrm{NL}}/I$ of about $26\,\Omega\,\mu\mathrm{m}^2$, with A the area of the injector tunnel contact. We further confirm the presence of spin accumulation in the Si channel by measuring the nonlocal Hanle effects in both P and AP configurations [Fig. 4(b)]. For the P state, we observe a reduction of V_{NL} from its maximum value due to spin precession in the external perpendicular magnetic field (B_z). A similar behavior is observed for the AP state with an opposite sign. The signal magnitude ($V_{\mathrm{NL}} \sim 0.19$ mV) agrees well with the spin-valve data, proving the creation of spin accumulation and the lateral spin transport in the Si channel.

To precisely determine the spin-diffusion length L_{SD}, we employ the same method as that described in Ref. [12]. We collect the conventional nonlocal spin-valve data for devices A, B, and C using either the narrow FM contact as the injector and the wider FM contact as the detector, or

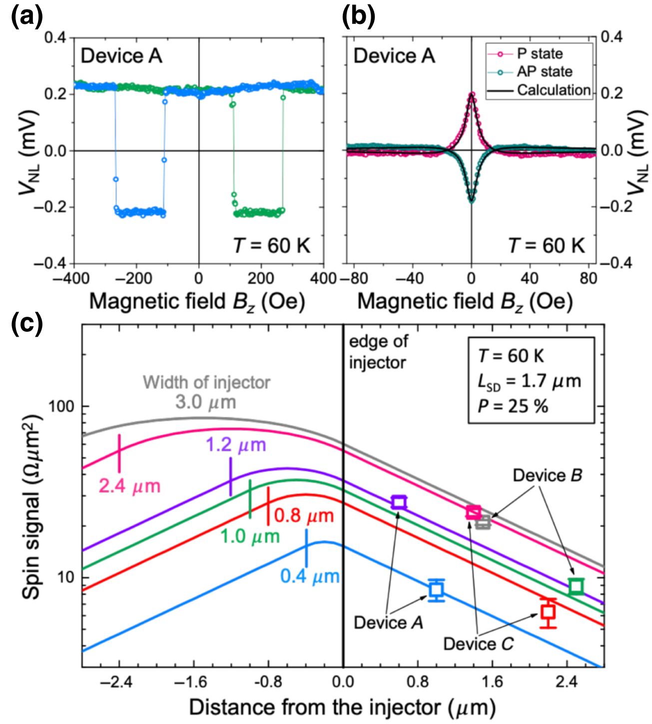

FIG. 4. (a) Nonlocal spin-valve signal and (b) Hanle spin signals for parallel (P) and antiparallel (AP) magnetization of injector and detector, measured at 60 K on device A using the 1.2- and 0.4-μm wide FM contact as the spin injector and detector, respectively. B_y and B_z are the external magnetic fields applied in-plane along the length of the FM contacts and perpendicular to the film plane, respectively. A constant tunnel current density J_T of 0.8 kA/cm^2 is applied to the injector contact and an offset voltage of approximately 3 mV is subtracted from the nonlocal signal measured across the detector junction. (c) Calculated spin signal vs position produced by the spin accumulation in the Si for different widths of the FM injector contact (solid lines) and experimental data (symbols) for devices A, B, and C obtained by using either the narrow FM strip as the injector and the wider FM strip as the detector, or vice versa. The tunnel current density ($J_T \sim 0.4$ kA/cm^2) is small enough to ensure that transport is by spin diffusion only. The injector is located between 0 (right edge) and $-W_{\mathrm{inj}}$ (left edge, indicated by the short colored vertical lines). The experimental data are compared to the calculated spin signal at the center of the detector, which is located to the right of the injector. The best agreement with the data is obtained using $L_{\mathrm{SD}} = 1.7\ \mu$m and $P_{\mathrm{inj}} = P_{\mathrm{det}} = P = 25\%$ in the calculation.

vice versa, with an identical tunnel current density J_T. A low current is used, ensuring that the electric field in the Si channel is negligible. We then calculate the spatial profile of the injected spin accumulation as a function of the injector width (W_{inj}) using numerical evaluation of the one-dimensional spin transport in the purely diffusive regime, as is done in Ref. [12]. Then we fit the experimental data by adjusting L_{SD} and the tunnel spin polarization P (assuming that $P_{\mathrm{inj}} = P_{\mathrm{det}} = P$ at low bias). As shown in Fig. 4(c), the magnitude of the nonlocal spin signals for different W_{inj} is well described by the numerical calculations of the spin-accumulation profile by taking $L_{SD} = 1.7\ \mu$m and $P \sim 25\%$ for Fe/MgO tunnel contacts. To obtain the spin lifetime τ_{sf}, we follow the procedure described in Ref. [12], fitting the Hanle curves in P and AP states with L_{SD} set to the predetermined value (1.7 μm). As shown in Fig. 4(b), good fits are obtained for $\tau_{sf} = 17$ ns, which is comparable to what was previously obtained [12] for devices with a similar doping concentration.

V. QUANTIFICATION OF SPIN DRIFT

To quantify the effect of spin drift, we compare the spin signals measured in the NL and XNL geometries under high bias conditions. Figure 5 shows typical spin-valve measurements performed on device A with a tunnel current density J_T across the injector interface of ± 4.2 kA/cm^2 ($I = \pm 2$ mA). Clear spin-valve signals are observed for both schemes. However, for $I = +2$ mA, the magnitude of the spin signal measured in the XNL configuration is larger than that for NL configuration, whereas for $I = -2$ mA, we observe the opposite ($V_{XNL} < V_{NL}$). These results are consistent with the expected effect of the electric field in the Si channel, as described above in Sec. II, specifically Eq. (4), which predicts $V_{XNL}/V_{NL} > 1$ for spin injection bias and $V_{XNL}/V_{NL} < 1$ for spin extraction bias.

Next, we examine the modulation of the spin-valve signals as a function of the strength of E. The field in the Si channel is given by $E = \rho_{Si} J_{Si} = \rho_{Si}\ (I/A_{Si})$ with J_{Si} the current density in the Si channel having a cross-section area of A_{Si}. Because $I \propto J_T\ W_{inj}$, the current density in the channel, and thus the drift electric field, can be varied either by increasing the tunnel current density or by increasing the injector width at constant J_T, as illustrated in Fig. 6. Thus, we measure the spin-valve signals as a function of the tunnel current density J_T in both the NL and the XNL configurations using injectors of different widths. The results are presented in Fig. 7 for injectors having a width varying from 0.4 to 3 μm. First, we observe that as J_T increases, V_{XNL} is gradually enhanced compared to V_{NL} for positive bias (spin injection), whereas a progressive reduction of V_{XNL} compared to V_{NL} occurs for negative bias (spin extraction). Second, the difference between V_{XNL} and V_{NL} becomes more and more pronounced as the width of the injector becomes larger. These two trends are in qualitative agreement with that expected for spin drift and the scaling of the drift electric field in the channel as a function of J_T and W_{inj}. It is worth noting that the spin signal for the XNL geometry is larger by a factor of about 2.5 for the 3-μm wide FM contact [Fig. 7(f)] in the large current regime, for which the corresponding electric field in the Si between the injector and detector is still rather moderate (400–800 V/cm). Hence, spin drift can indeed significantly enhance spin signals compared to purely diffusive spin transport, even in a heavily doped semiconductor.

To extract the spin-transport length $L(E)$ as a function of E, we plot the ratio V_{XNL}/V_{NL} as a function of J_T for each injector width and fit the experimental data with Eqs. (2) and (4) with only ε_d as a free parameter (Fig. 8). By setting ε_d equal to 39 meV, a good fit is obtained simultaneously for all the six data sets. Hence, the observed trends are well described by the theory for spin drift. Note, however, that the measured ratio V_{XNL}/V_{NL} is lower than expected for very large spin injection conditions [Figs. 8(e) and 8(f)

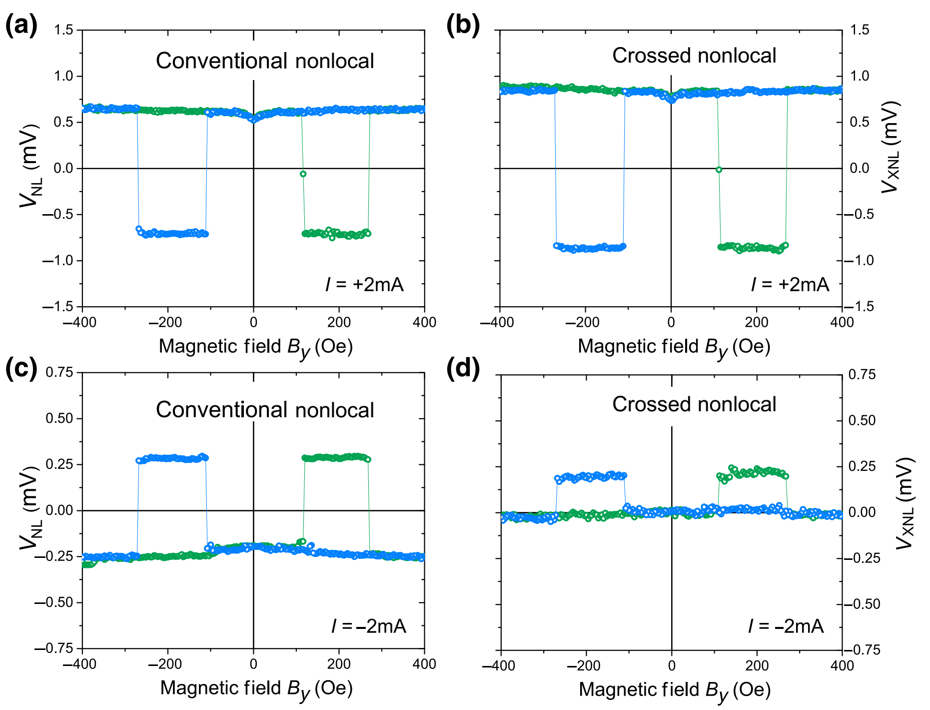

FIG. 5. Nonlocal spin-valve signals measured using the conventional measurement configurations (left panels), and the crossed configuration (right panels). For panels (a) and (b), a current I of $+2$ mA ($J_T \sim 4.2$ kA/cm^2) is applied to the injector contact and an offset voltage of $+13$ mV is subtracted from the detected signal. For panels (c) and (d), a current I of -2 mA ($J_T \sim -4.2$ kA/cm^2) is applied through the injector contact and an offset voltage of -13 mV is subtracted from the detected signal. The measurements are performed at 60 K on device A using the 1.2 and 0.4 μm wide FM contacts as the spin injector and detector, respectively. Note that the spin signal is larger for the positive injector current, because for that polarity, the spin polarization of the injected current is larger than for negative injection bias, as previously reported [17].

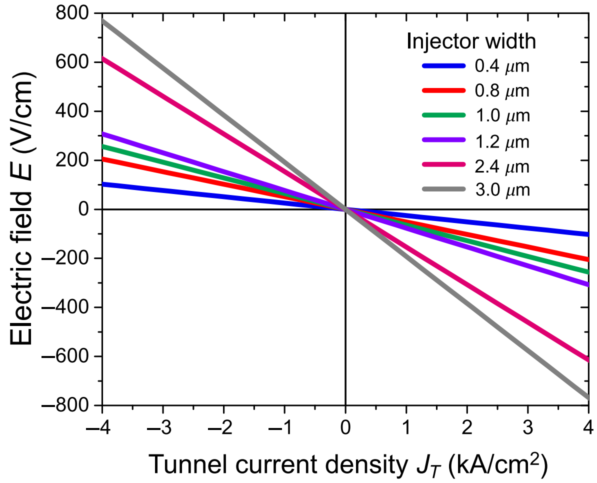

FIG. 6. Calculated value of the electric field E in the Si channel as a function of the tunnel current density J_T in the injector contact, for injectors having different widths W_{inj}.

for channel current density J_{Si} >50 kA/cm^2]. Although the precise origin of this discrepancy is unclear, the deviation occurs for devices having an injector width (2.4 and 3 μm) that is larger than the spin-diffusion length (1.7 μm). The line injector model, which we use to derive Eq. (4), is accurate only for $W_{\mathrm{inj}} < L_{\mathrm{SD}}$ (see Ref. [12]), and this may contribute to the discrepancy. From the determined value of ε_d, we compute the spin-transport length as a function of E using Eq. (2). The result is shown in Fig. 9. For an electric field of $E = \pm 400$ V/cm, the characteristic spin-transport length is increased or decreased by about a factor of two compared to the spin-diffusion length. Hence, spin drift can significantly change the spin transport in heavily doped Si. A similar set of data obtained at 150 K confirms this (see the Supplemental Material [27]).

To complete the quantitative analysis, we compare the experimentally determined value of ε_d to that predicted by the theory developed in Refs. [18,19] for spin drift, which says that $\varepsilon_d = eD/\mu$. From the nonlocal spin-valve and Hanle measurements presented in Sec. IV, the values of L_{SD} (1.7 μm) and τ_{sf} (17 ns) are obtained. Using these experimental values, we obtain the diffusion constant of electrons in the Si channel as $D = L_{\mathrm{SD}}^2/\tau_{\mathrm{sf}} =$ 1.7 cm^2/s at 60 K. With the measured electron mobility of the Si substrate at 60 K ($\mu = 147$ cm^2/V s), the theory predicts that $\varepsilon_d = eD/\mu = 11.6$ meV. This is more than three times smaller than the value (39 meV) extracted directly from our data. Since the effect of spin drift

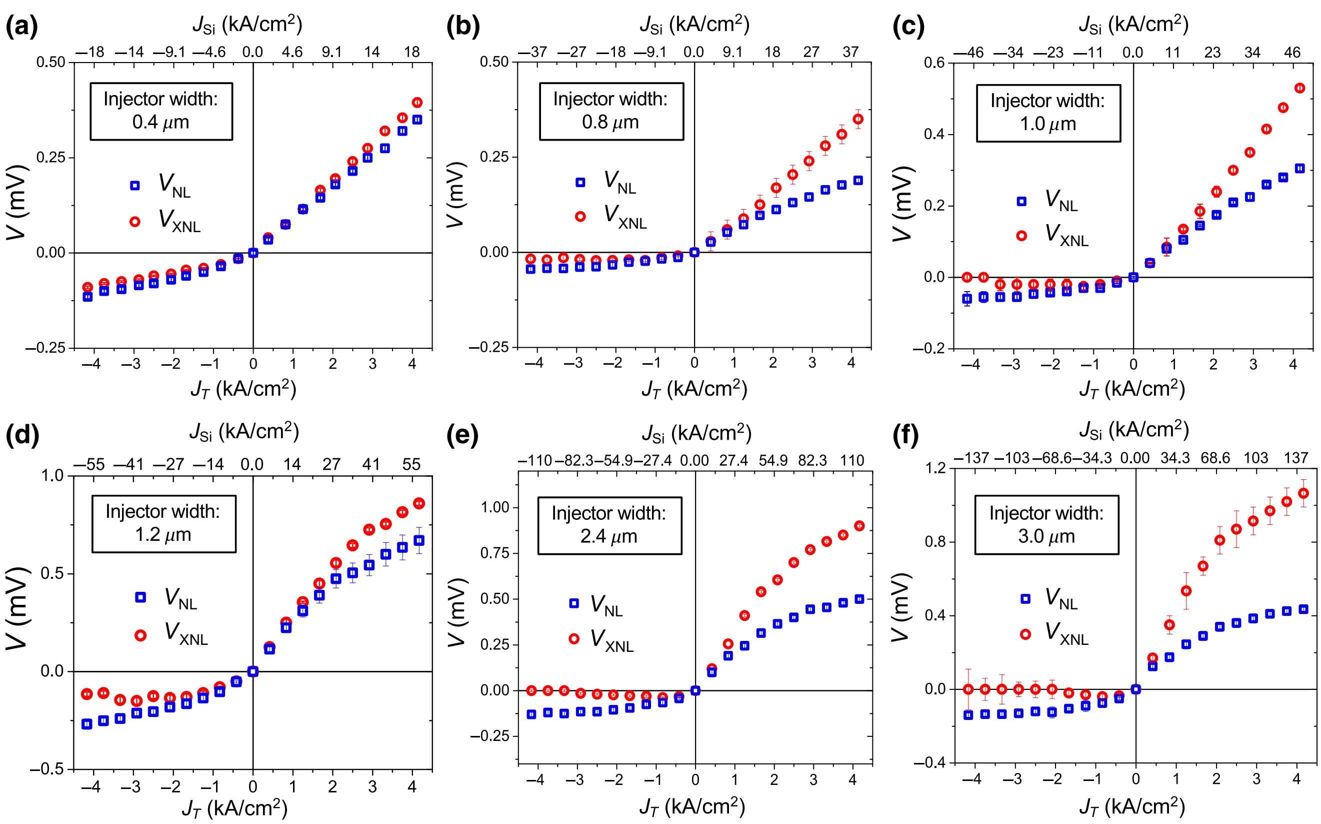

FIG. 7. Comparison of the nonlocal spin signals measured in the conventional configuration (V_{NL}, dark blue squares) and in the crossed configuration (V_{XNL}, red circles) as a function of the current density J_T in the injector contact (bottom x axis). The corresponding current density J_{Si} in the Si channel is also indicated (top x axis). Measurements are performed at 60 K for six different widths of the injector contact, as indicated.

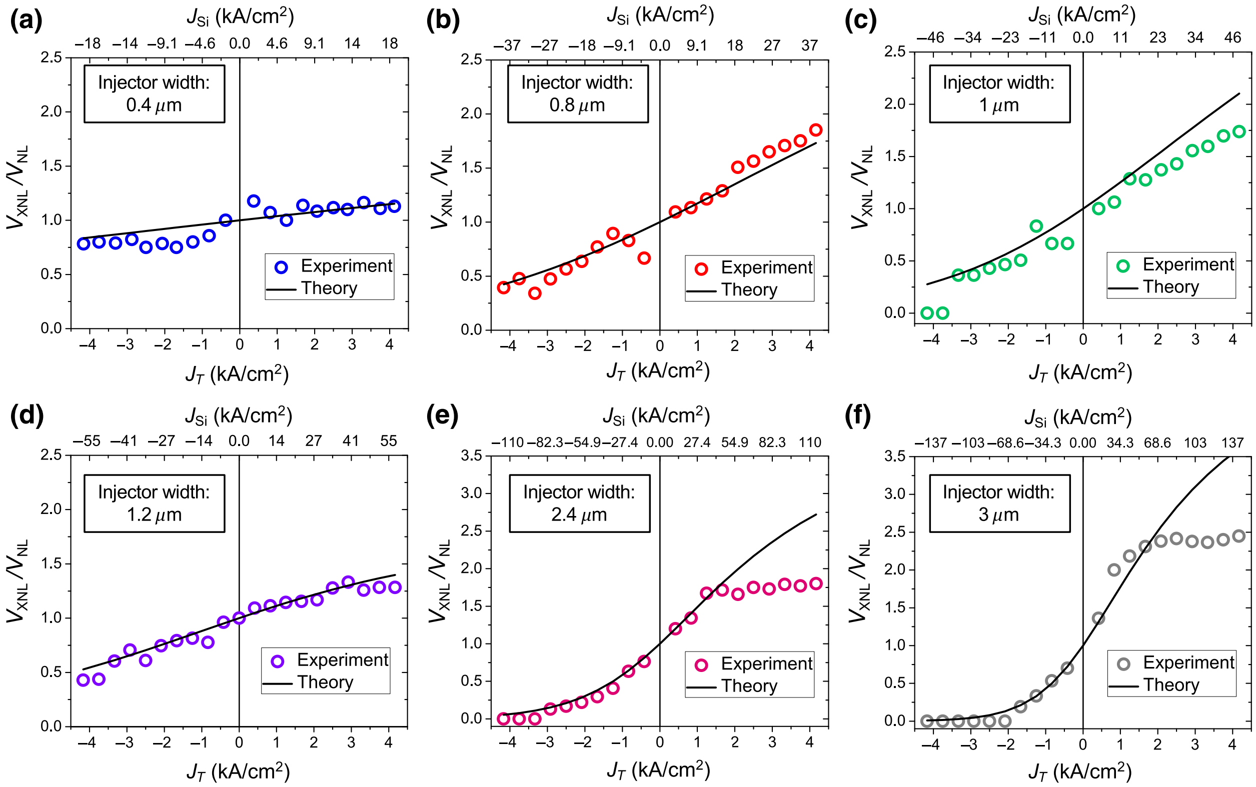

FIG. 8. Ratio V_{XNL}/V_{NL} of the spin signals in the XNL measurement configuration and the conventional NL configuration as a function of the current density J_T in the injector contact (bottom x axis). The corresponding current density J_{Si} in the Si channel is also indicated (top x axis). The open circles correspond to the experimental data, extracted from Fig. 7, whereas the solid lines correspond to the fit using Eqs. (2) and (4).

becomes stronger when ε_d is smaller, the theory significantly overestimates the effect of spin drift. In fact, if we use the theory value of $\varepsilon_d = 11.6$ meV, the predicted spin-transport length changes much more rapidly as a function of E as compared to the actual length scale derived from the experiment (see Fig. 9). The difference might be caused by the description [18,19] of a heavily doped semiconductor using textbook expressions for a degenerate semiconductor, as this does not take into account the impurity band conduction that is known to occur in heavily doped semiconductors [29].

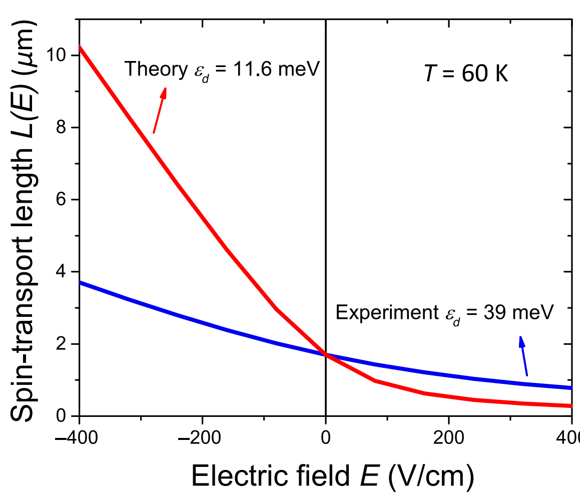

FIG. 9. Spin-transport length $L(E)$ as a function of the electric field E in the Si channel, as computed from Eq. (2) using the energy scale $\varepsilon_d = 39$ meV extracted from the experimental data (blue curve). The red curve shows the spin-transport length predicted by the theory using $\varepsilon_d = 11.6$ meV.

VI. EFFECT OF SPIN DRIFT ON THE CONVENTIONAL NONLOCAL SPIN SIGNAL

It is generally assumed that in the conventional nonlocal geometry, the nonlocal spin signal is not affected by spin drift because there is no electric field in the detector circuit or in the channel between the injector and detector. We argue here that this is not correct, because the electric field in the channel can only displace the spin accumulation into a certain direction, but it cannot create extra spins or annihilate spins. The total spin density, integrated over the complete volume of the channel, is determined by the injected spin current and the rate of spin relaxation in the channel. Now, if we start from a purely diffusive situation and then include the electric field in the injector circuit, the change in the spin-transport length in the

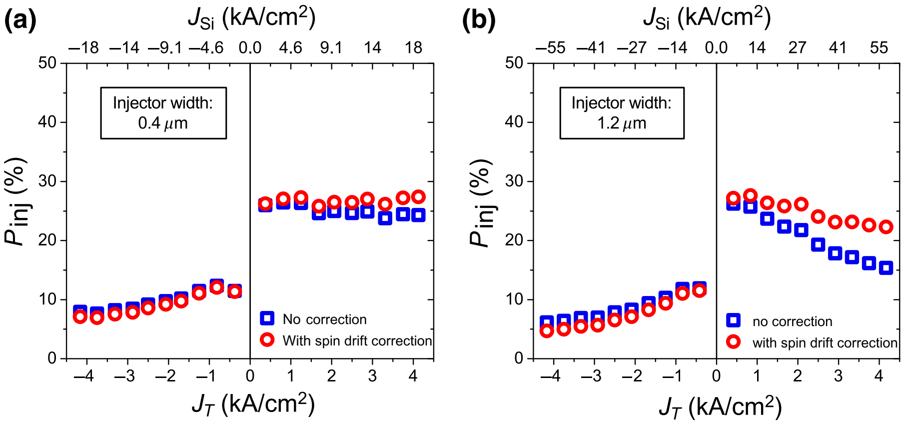

FIG. 10. Spin polarization (P_{inj}) of the injected tunnel current as a function of the tunnel current density J_T calculated from the conventional nonlocal spin-valve signals in two different ways: (i) using Eq. (3), which does not take spin drift in the injector circuit into account (blue square symbols), or (ii) using Eq. (6), which includes the correction for spin drift (red circles). Measurements are performed at 60 K on device A for (a) the 0.4-μm wide contacts as the spin injector, or for (b) the 1.2-μm wide FM contact as the spin injector.

injector circuit would cause the integrated spin density to change. Since this cannot happen, an overall renormalization of the spin accumulation has to occur to compensate. Or, in other words, the electric field in the injector circuit causes a redistribution of the spin density everywhere in the channel, including on the side of the nonlocal detector. Hence, the nonlocal spin signal V_{NL} is a function of E, even though the electric field is present only in the injector circuit.

The renormalization factor can be obtained by requiring that the total spin density, integrated over the complete channel, is the same with and without the electric field. This is easily done in the line injector approximation model ($W_{\mathrm{inj}} < L_{\mathrm{SD}}$), for which the spin density decays away from the center of the injector contact in an exponential way. On the side where $E = 0$, the decay length is L_{SD}, whereas the decay length is $L(E)$ on the side where the electric field is present. For purely diffusive transport, the integration produces a value of $\Delta\mu^0\ L_{\mathrm{SD}}$ on both sides of the injector center, and thus a total of $\Delta\mu^0\ (2\ L_{\mathrm{SD}})$, where $\Delta\mu^0$ is the magnitude of the spin accumulation at the center of the injector in the absence of spin drift. If spin drift is included, the integration yields $\Delta\mu(E)L(E)$ on one side and $\Delta\mu(E)L_{\mathrm{SD}}$ on the other side, and thus a total of $\Delta\mu(E)\ [L_{\mathrm{SD}} + L(E)]$, where $\Delta\mu(E)$ is the renormalized magnitude of the spin accumulation at the center of the injector in the presence of spin drift. We then obtain for the renormalization

$$\Delta\mu(E) = \Delta\mu^0 \left(\frac{2L_{\mathrm{SD}}}{L_{\mathrm{SD}} + L(E)} \right). \tag{5}$$

In the presence of spin drift in the injector circuit, the nonlocal spin signal in the conventional geometry is then given by

$$V_{\mathrm{NL}}(E) = \left(\frac{2L_{\mathrm{SD}}}{L_{\mathrm{SD}} + L(E)} \right) P_{\mathrm{inj}} P_{\mathrm{det}} J_T \rho_{\mathrm{Si}} L_{\mathrm{SD}} \left(\frac{W_{\mathrm{inj}}}{2t_{\mathrm{Si}}} \right) \exp\left(\frac{-d_c}{L_{\mathrm{SD}}} \right). \tag{6}$$

At $E = 0$, we have $L(E) = L_{\mathrm{SD}}$, thus the renormalization factor is equal to 1. If the injector is biased in spin injection mode, $L(E) > L_{\mathrm{SD}}$ and the spin accumulation under the detector and thus V_{NL} are reduced by the spin drift in the injector circuit. For spin extraction bias, the spin accumulation under the detector is enhanced by the spin drift in the injector circuit. Note that the renormalization factor is the same for the XNL geometry, and thus does not appear in the ratio in Eq. (4).

We now show how the renormalization affects the value of the spin polarization P_{inj} of the injected current that is extracted from the amplitude of the conventional nonlocal spin signal. Figure 10 displays the extracted value of the spin polarization for two different contacts (0.4 and 1.2 μm wide, respectively). As the bias current becomes larger, the spin polarization extracted without taking spin drift into account, using Eq. (3), deviates significantly from the correct value of the spin polarization that is obtained when the renormalization due to spin drift in the injector circuit is taken into account, using Eq. (6). Taking spin drift into account increases the extracted value of P_{inj} for positive (spin injection) bias and reduces it for negative (spin extraction) bias. The deviation is more pronounced for the wider contact, because for a wider contact, the same tunnel current density produces a larger current in the Si channel, and thus a larger drift electric field. We conclude that, in general, spin drift needs to also be taken into account for the conventional nonlocal geometry. However, spin drift does not need to be taken into account when the spin-diffusion length is determined from the decay of the spin signal as a function of the distance d_c between injector and detector, as this decay is governed by L_{SD}, although care has to be taken that the same injector current (same E) is used for devices with different d_c, so as to ensure that the renormalization factor is the same for all devices.

VII. CONCLUSION

In conclusion, the effect of a drift electric field on the spin transport in heavily doped Si is quantified using a simple and reliable method that is based on the ratio of the spin-valve signals in the conventional nonlocal and the crossed-nonlocal measurement geometries. The spin-transport length $L(E)$ is obtained as a function of the drift electric field, and it is found that drift electric fields of ± 400 V/cm modify the spin-transport length (either up or down) by about a factor of two, relative to L_{SD}. The observed trends are in agreement with the theory for spin drift. However, the energy scale ε_d predicted by the theory is smaller by more than a factor of three compared to the actual value extracted from the data, implying that the theory significantly overestimates the effect of spin drift. It is also shown that in the conventional nonlocal spin-transport configuration, in which there is no electric field between the injector and the detector contact, spin drift nevertheless modifies the magnitude of the spin accumulation under the nonlocal detector. We, therefore, introduce a spin drift correction factor for nonlocal devices, which allows correct parameters to be extracted from data taken at higher bias currents.

ACKNOWLEDGMENTS

This work was supported by the Grant-in-Aid for Scientific Research on Innovative Areas, Nano Spin Conversion Science (Grants No. 26103002 and No. 26103003).

[1] I. Žutić, J. Fabian, and S. Das Sarma, Spintronics: Fundamentals and applications, Rev. Mod. Phys. **76**, 323 (2004).

[2] J. Fabian, A. Matos-Abiague, C. Ertler, P. Stano, and I. Žutić, Semiconductor spintronics, Acta Phys. Slovaca **57**, 565 (2007).

[3] A. Fert, Nobel Lecture: Origin, development, and future of spintronics, Rev. Mod. Phys. **80**, 1517 (2008).

[4] S. Sugahara and J. Nitta, Spin-transistor electronics: An overview and outlook, Proc. IEEE **98**, 2124 (2010).

[5] R. Jansen, Silicon spintronics, Nat. Mater. **11**, 400 (2012).

[6] R. Jansen, S. P. Dash, S. Sharma, and B. C. Min, Silicon spintronics with ferromagnetic tunnel devices, Semicond. Sci. Technol. **27**, 083001 (2012).

[7] O. M. J. van't Erve, A. T. Hanbicki, M. Holub, C. H. Li, C. Awo-Affouda, P. E. Thompson, and B. T. Jonker, Electrical injection and detection of spin-polarized carriers in silicon in a lateral transport geometry, Appl. Phys. Lett. **91**, 212109 (2007).

[8] S. P. Dash, S. Sharma, R. S. Patel, M. P. de Jong, and R. Jansen, Electrical creation of spin polarization in silicon at room temperature, Nature **462**, 491 (2009).

[9] T. Suzuki, T. Sasaki, T. Oikawa, M. Shiraishi, Y. Suzuki, and K. Noguchi, Room-temperature electron spin transport in a highly doped Si channel, Appl. Phys. Express **4**, 023003 (2011).

[10] M. Shiraishi, Y. Honda, E. Shikoh, Y. Suzuki, T. Shinjo, T. Sasaki, T. Oikawa, K. Noguchi, and T. Suzuki, Spin transport properties in silicon in a nonlocal geometry, Phys. Rev. B **83**, 241204 (2011).

[11] M. Ishikawa, T. Oka, Y. Fujita, H. Sugiyama, Y. Saito, and K. Hamaya, Spin relaxation through lateral spin transport in heavily doped n-type silicon, Phys. Rev. B **95**, 115302 (2017).

[12] A. Spiesser, H. Saito, Y. Fujita, S. Yamada, K. Hamaya, S. Yuasa, and R. Jansen, Giant Spin Accumulation in Silicon Nonlocal Spin-Transport Devices, Phys. Rev. Appl. **8**, 064023 (2017).

[13] P. M. Tedrow and R. Meservey, Spin-Dependent Tunneling into Ferromagnetic Nickel, Phys. Rev. Lett. **26**, 192 (1971).

[14] R. Meservey and P. M. Tedrow, Spin-polarized electron tunneling, Phys. Rep. **238**, 173 (1994).

[15] M. Johnson and R. H. Silsbee, Interfacial Charge-Spin Coupling: Injection and Detection of Spin Magnetization in Metals, Phys. Rev. Lett. **55**, 1790 (1985).

[16] A. Fert and H. Jaffrès, Conditions for efficient spin injection from a ferromagnetic metal into a semiconductor, Phys. Rev. B **64**, 184420 (2001).

[17] R. Jansen, A. Spiesser, H. Saito, Y. Fujita, S. Yamada, K. Hamaya, and S. Yuasa, Nonlinear Electrical Spin Conversion in a Biased Ferromagnetic Tunnel Contact, Phys. Rev. Appl. **10**, 064050 (2018).

[18] Z. G. Yu and M. E. Flatté, Electric-field dependent spin diffusion and spin injection into semiconductors, Phys. Rev. B **66**, 201202 (2002).

[19] Z. G. Yu and M. E. Flatté, Spin diffusion and injection in semiconductor structures: Electric field effects, Phys. Rev. B **66**, 235302 (2002).

[20] C. Jozca, M. Popinciuc, N. Tombros, H. T. Jonkman, and B. J. van Wees, Electronic Spin Drift in Graphene Field-Effect Transistors, Phys. Rev. Lett. **100**, 236603 (2008).

[21] S. A. Crooker, E. S. Garlid, A. N. Chantis, D. L. Smith, K. S. M. Reddy, Q. O. Hu, T. Kondo, C. J. Palmstrøm, and P. A. Crowell, Bias-controlled sensitivity of ferromagnet/semiconductor electrical spin detectors, Phys. Rev. B **80**, 041305 (2009).

[22] T. A. Peterson, S. J. Patel, C. C. Geppert, K. D. Christie, A. Rath, D. Pennachio, M. E. Flatté, P. M. Voyles, C. J. Palmstrøm, and P. A. Crowell, Spin injection and detection up to room temperature in Heusler alloy/n -GaAs spin valves, Phys. Rev. B **94**, 235309 (2016).

[23] T. Sasaki, Y. Ando, M. Kameno, T. Tahara, H. Koike, T. Oikawa, T. Suzuki, and M. Shiraishi, Spin Transport in Nondegenerate Si with a Spin MOSFET Structure at Room Temperature, Phys. Rev. Appl. **2**, 034005 (2014).

[24] T. Tahara, Y. Ando, M. Kameno, H. Koike, K. Tanaka, S. Miwa, Y. Suzuki, T. Sasaki, T. Oikawa, and M. Shiraishi, Observation of large spin accumulation voltages in nondegenerate Si spin devices due to spin drift effect: Experiments and theory, Phys. Rev. B **93**, 214406 (2016).

[25] M. Kameno, Y. Ando, T. Shinjo, H. Koike, T. Sasaki, T. Oikawa, T. Suzuki, and M. Shiraishi, Spin drift in highly doped n-type Si, Appl. Phys. Lett. **104**, 092409 (2014).

[26] In Ref. 25, the presence of spin drift in heavily doped Si was convincingly demonstrated by a qualitative comparison of the spin-valve signals in NL and XNL geometries. However, for quantitative analysis, the authors used the nonlocal Hanle signal, which is not reliable, as we point out in the Supplemental Information [27]. Even in the conventional NL geometry, a large bias current is shown to produce a difference in the amplitude of the Hanle curves for parallel

and antiparallel magnetic configurations, and also a significant broadening. This cannot be explained by spin drift, and indicates that additional effects are at play. These cannot be subtracted in a simple manner. Therefore, quantitative analysis of spin drift using Hanle measurements at large bias current is not an appropriate method.

[27] See Supplemental Material at http://link.aps.org/supplemental/10.1103/PhysRevApplied.11.044020 for a discussion of the complications in quantifying spin drift from Hanle curves, and for additional data taken at 150 K.

[28] M. Kameno, Y. Ando, E. Shikoh, T. Shinjo, T. Sasaki, T. Oikawa, Y. Suzuki, T. Suzuki, and M. Shiraishi, Effect of spin drift on spin accumulation voltages in highly doped silicon, Appl. Phys. Lett. **101**, 122413 (2012).

[29] E. M. Conwell, Impurity band conduction in germanium and silicon, Phys. Rev. **103**, 51 (1956).